Supporting Information

Asner et al. 10.1073/pnas.0810637106

SI Materials and Methods

Remote-Sensing System. Large-scale analysis of forest 3-D structure and biological composition requires a combination of advanced airborne imaging technologies that simultaneously resolve the horizontal and vertical characteristics of the vegetation, as well as the type of vegetation. No airborne (or space-based) technologies were available to make these simultaneous measurements, so we developed the CAO, a new system designed specifically for mapping the biochemical, taxonomic, and structural properties of vegetation and ecosystems (http://cao.stanford.edu) (1). The CAO combines 3 major instrument subsystems—HiFIS, waveform LiDAR scanner, and global positioning system–inertial measuring unit (GPS-IMU)—into a single airborne package.

The CAO HiFIS subsystem provides spectroscopic images of the land surface. The CAO-Alpha configuration uses a pushbroom imaging array with 1500 cross-track pixels, with sampling done across the 367–1058 nm range at a spectral resolution of up to 2.4 nm. The spectrometer subsystem is fully integrated with a waveform LiDAR subsystem with an adjustable laser pulse repetition rate of up to 100 kHz (1). The GPS-IMU subsystem provides 3-D positioning and attitude data for the sensor package on board the aircraft, allowing for highly precise and accurate projection of HiFIS and LiDAR observations on the ground (1). The CAO-Alpha configuration provides coaligned HiFIS and LiDAR data at a spatial resolution of 0.4–1.0 m, depending on the aircraft's altitude above the ground.

Airborne Data Collection. In April–May 2008, we operated the CAO-Alpha system over KNP. The CAO-Alpha data were collected at 1,000 m above ground level, providing combined HiFIS and LiDAR measurements at a spatial resolution of 56 cm. All flights were conducted within 2.5 h of solar noon. For this study, the airborne data were collected over 790 ha of herbivore enclosure-exclosure areas and an additional 850 ha of surrounding savanna region.

Data Processing and Analysis. Fusion of the imaging spectroscopy and LiDAR data requires a processing stream that maximizes the sharing of information between data products. Given the enormous data volumes involved, the processing stream must be highly automated. Fig. S2 shows the processing stream for this study, in which raw spectral, laser, and trajectory data are integrated and analyzed in a series of higher-order products and results. The following sections briefly describe the major steps in the process.

Aircraft Positioning. The CAO uses in-flight and postflight data integration approaches to precisely match HiFIS and LiDAR data in 3-D space. The in-flight step is achieved by providing a common mount with measured offsets between instrument optical centers, as well as time-stamping of spectral and LiDAR data collection streams with shared position and trajectory data. The LiDAR has a custom-designed laser beam divergence to precisely match the field of view of the CAO-Alpha spectrometer. The GPS-IMU data provide the common link for the detailed ray-tracing of the photons between aircraft sensors and the ground. The point-for-point alignment of the LiDAR and HiFIS data are complicated by inherent differences in the scanning geometries of the 2 systems and further distortions of the ground sampling grid due to topography. Our approach is to recover the best estimates for each pixel center location in 3 dimensions for both the LiDAR and HiFIS data (1), then use these pixel centers to render the 2 data sets into a single, integrated grid of HiFIS and LiDAR data for subsequent processing, analysis, and product generation.

LiDAR Data Processing. The GPS-IMU data are combined with the laser ranging data to determine the 3-D location of the laser returns. From the laser "point cloud" data, a physical model is used to estimate top-of-canopy and ground surfaces [digital elevation models (DEMs)], using the REALM (Optech) and Terrascan/Terramatch (Terrasolid) software packages. Vegetation height is then estimated by differencing the top-of-canopy and ground surface DEMs (2, 3).

HiFIS Data Processing. The HiFIS data are converted to at-sensor radiances by applying radiometric corrections developed during sensor calibration in the laboratory. Apparent surface reflectance is then derived from the radiance data using an automated atmospheric correction model (ACORN 5LiBatch; Imspec). Inputs to the atmospheric correction algorithm include ground elevation (from the LiDAR), aircraft altitude (from GPS-IMU), solar and viewing geometry, atmosphere type (e.g., tropical), and estimated visibility (in km). The code uses a MODTRAN look-up table to correct for Rayleigh scattering and aerosols. Water vapor is estimated directly from the 940-nm water vapor feature in the radiance data.

Once the HiFIS and LiDAR data have been prepared, the spectral images are masked based on illumination conditions between the sensors and canopies (Fig. S2). The LiDAR and GPS-IMU data provide 3-D maps of precise illumination conditions on each canopy, allowing for the automatic identification and masking of shaded portions of the vegetation.

The masked HiFIS images are passed to an automated spectral mixture analysis model, AutoMCU (4). This algorithm uses spectroscopic signatures to quantify the fractional cover of PV, NPV, and bare substrate within each image pixel, and Monte Carlo unmixing to derive mean estimates of fractional cover along with standard deviation and root mean squared error data on a per-pixel basis.

Landscape Stratification. Savanna landscapes are heterogeneous systems in both space and time (5, 6), so careful consideration must to be given to landscape stratification for analysis purposes. Catenal development (7), whereby soil and vegetation associations vary down slope, is evident throughout much of KNP (8). The distinction between the nutrient-poor sandy soils of the upland positions and the more nutrient-rich clay soils of the lowland positions provides an ecologically meaningful basis upon which to dissect the landscape.

High-resolution (56 cm) DEMs, derived from the LiDAR data, were used in conjunction with available soil maps (KNP GIS database; http://www.sanparks.org/parks/kruger/conservation/scientific/gis/gisrsdataview.php) to delineate upland and lowland patch types at each site in both protected and accessible areas. From within each of these patches, the most comparable areas of similar size were selected based on topography. Comparisons between the herbivore exclusion treatments and the accessible areas at each site were conducted on a patch-specific basis.

At Nkuhlu and Letaba, 2 different exclosure types are present: full exclosure, consisting of mesh fencing that excludes all herbivores larger than hares, and partial exclosure, consisting of 2 strands of wire that exclude only elephants and giraffes. For the purposes of this analysis, only the full exclosures were sampled with their respective accessible areas, because these are more

similar to the design of the longer-term sites, where mesh fencing is also used.

Whereas both of the long-term sites are burned in conjunction with the KNP fire management policy, fire is excluded from half of the treatment area at the short-term sites, with the other half is allowed to burn under natural conditions. Since its establishment, no fires have occurred at the Letaba site, but the southern portion of the full exclosure at Nkuhlu was burned in 2007. We sampled only the nonburned areas in our analysis, to remove fire as a covariate.

Statistical Analysis. After identifying the most suitable areas for our comparisons, we further subsampled them (66% of the smallest region of interest), to dampen the potential influences of spatial autocorrelation. This procedure resulted in the random sampling of 27,000 pixels (summing to 8,467 m^2) in both upland and lowland hillslope positions, with and without herbivores at each of the 4 sites. Statistical differences in vegetation 3-D structure and fractional cover were determined using the K-S test. This nonparametric test is well suited to such analyses, because it is sensitive to differences in both the location and shape of the empirical cumulative distribution functions (9). We also pooled data from different areas to evaluate the general effects of herbivore presence/absence independent of substrate. Comparisons of means for protected and unprotected areas were conducted using standard t tests. We considered this approach to be robust because of the near-normal nature of the data and the large sample size.

Field Validation of Airborne Vegetation Heights and Fractional Cover. LiDAR-derived vegetation height from the CAO was validated in forested settings in previous work (10), but had yet to be evaluated in a semiarid savanna system. Thus, we carried out a field campaign to assess the accuracy of the vegetation height estimates in KNP. We collected 350 randomly selected field points for woody canopies ranging in height from 1 to 16 m and including a wide range of the common plant species found throughout the park. The data were collected with an extendable, graduated range pole or a handheld laser range finder (Impulse200; Laser Technologies). The geographic coordinate of each point was logged on a survey-grade GPS receiver (GeoXT; Trimble) and later differentially corrected to submeter accuracy using a local GPS base station (http://www.trignet.co.za/). The individual tree crowns of the field-measured trees were digitized as polygons in the LiDAR-derived canopy height model. The maximum canopy height for each polygon was then calculated and regressed against the field data for that particular tree. Linear regression indicated a strong positive relationship between field-measured and remotely sensed vegetation height (Fig. S3), with $r^2 = 0.92$, $P < .01$, and a standard error of the estimate of 1.17 m.

Fractional canopy cover mapping methods have been heavily validated in previous studies across a range of arid to humid ecosystems (4, 11–13); however, the imaging sensors used in those studies covered a broader range of the solar-reflected spectrum that incorporated the shortwave infrared (SWIR; 1300–2500 nm). Because the CAO HiFIS system does not extend past 1064 nm, we measured fractional cover in the field to validate the AutoMCU results in the absence of SWIR. We sampled 7 field transects ≈1 km in length. Fractional cover was visually classified as PV, NPV, or bare ground on a patch-by-patch basis (11). The locations of the leading and trailing edges of each patch were recorded with the GPS, and the points were later differentially corrected to submeter accuracy for comparison against the outputs from AutoMCU. We used a simple classification accuracy technique in which lateral cover estimates from spectral unmixing were considered to be correct for each patch when the field declaration matched the spectral unmixing classification. Despite the lack of SWIR coverage, we achieved an overall classification accuracy of 74%, derived from 658 patches across the 7 transects.

1. Asner GP, et al. (2007) Carnegie Airborne Observatory: In-flight fusion of hyperspectral imaging and waveform light detection and ranging (LiDAR) for three-dimensional studies of ecosystems. *J Appl Remote Sens* 1:DOI:10.1117/1111.2794018.
2. Lefsky MA, et al. (1999) LiDAR remote sensing of the canopy structure and biophysical properties of Douglas-fir western hemlock forests. *Remote Sensing of Environment* 70:339–361.
3. Lefsky MA, Cohen WB, Parker GG, Harding DJ (2002) LiDAR remote sensing for ecosystem studies. *BioScience* 52:19–30.
4. Asner GP, Heidebrecht KB (2002) Spectral unmixing of vegetation, soil and dry carbon cover in arid regions: Comparing multispectral and hyperspectral observations. *Int J Remote Sens* 23:3939–3958.
5. Belsky AJ (1995) Spatial and temporal landscape patterns in arid and semi-arid African savannas. *Mosaic Landscapes and Ecological Processes*, eds Hansson L, Fahrig L, Merriam G (Chapman & Hall, London), pp 31–56.
6. Pickett STA, Cadenasso ML, Benning TL (2003) Biotic and abiotic variability as key determinants of savanna heterogeneity at multiple spatiotemporal scales. *The Kruger Experience: Ecology and Management of Savanna Heterogeneity*, eds du Toit JT, Biggs HC, Rogers KH (Island Press, Washington, DC), pp 23–40.
7. Milne G (1935) Some suggested units of classification and mapping, particularly for east African soils. *Soil Res* 4:183–198.
8. Venter FJ, Scholes RJ, Eckhardt HC (2003) The abiotic template and its associated vegetation patten. *The Kruger Experience: Ecology and Management of Savanna Heterogeneity*, eds du Toit JT, Biggs HC, Rogers KH (Island Press, Washington DC), pp 83–129.
9. Sokal R, Rohlf F (1995) *Biometry: The Principles and Practice of Statistics in Biological Research* (WH Freeman, New York), 3rd Ed.
10. Asner GP, et al. (2008) Invasive plants transform the 3-D structure of rainforests. *Proc Natl Acad Sci U S A* 105:4519–4523.
11. Varga TA, Asner GP (2008) Hyperspectral and LiDAR remote sensing of fire fuels in Hawaii Volcanoes National Park. *Ecol Appl* 18:613–623.
12. Asner GP, Elmore AJ, Hughes FR, Warner AS, Vitousek PM (2005) Ecosystem structure along bioclimatic gradients in Hawai'i from imaging spectroscopy. *Remote Sens Environ* 96:497–508.
13. Harris AT, Asner GP (2003) Grazing gradient detection with airborne imaging spectroscopy on a semi-arid rangeland. *J Arid Environ* 55:391–404.

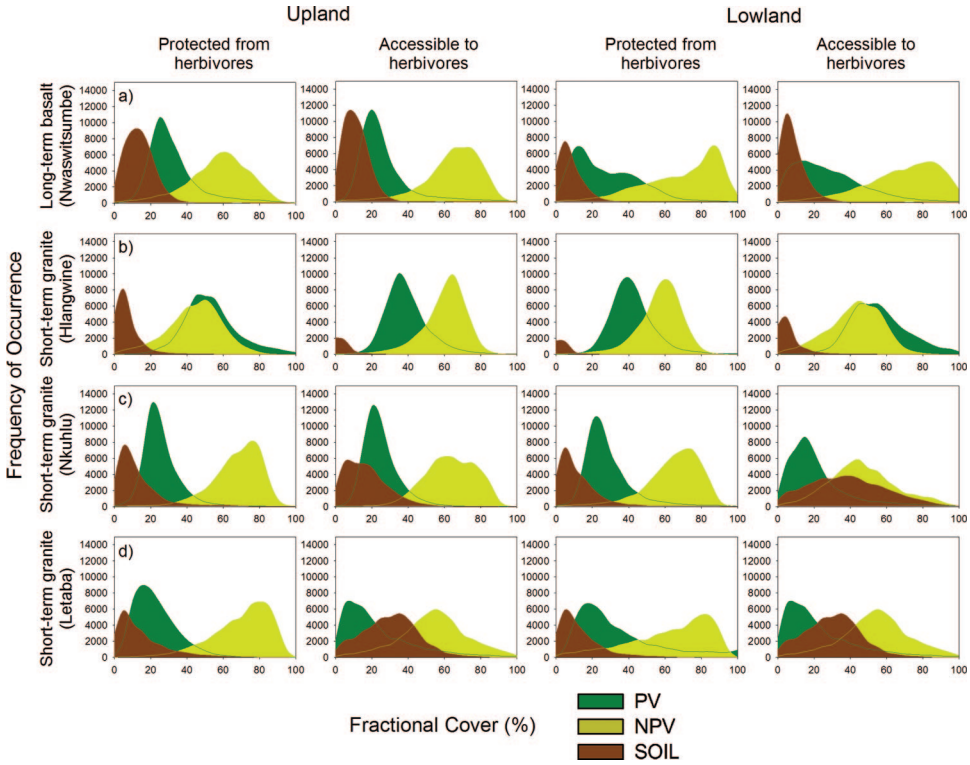

Fig. S1. Frequency histograms of live PV, dead/senescent NPV, and bare soil for upland and lowland areas protected from or accessible to herbivores. (*A* and *B*) Long-term treatment areas. (*C* and *D*) Short-term treatment areas. In all panels, the left columns are for uplands and the right columns are for lowlands. All comparisons between treatments were statistically different using the K-S test ($P < .01$).

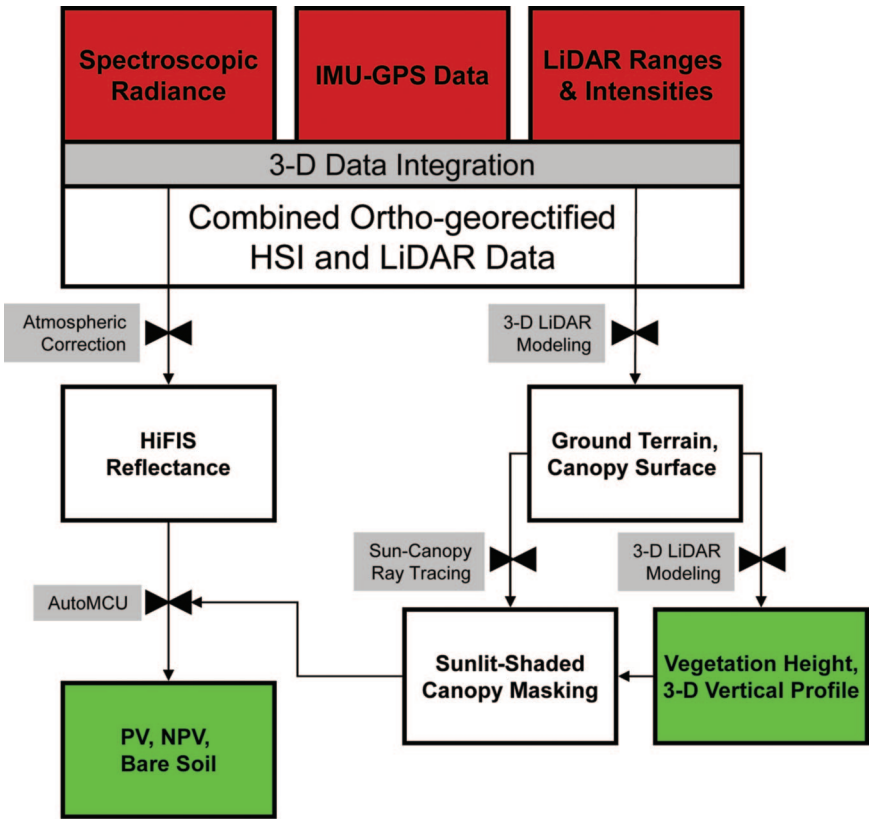

Fig. S2. The processing stream for in-flight and postflight integration of airborne imaging spectrometry and LiDAR observations, shade masking, and fractional canopy cover mapping. Raw data inputs from the CAO are shown in red; computer algorithms are depicted in gray. Final outputs are shown in green.

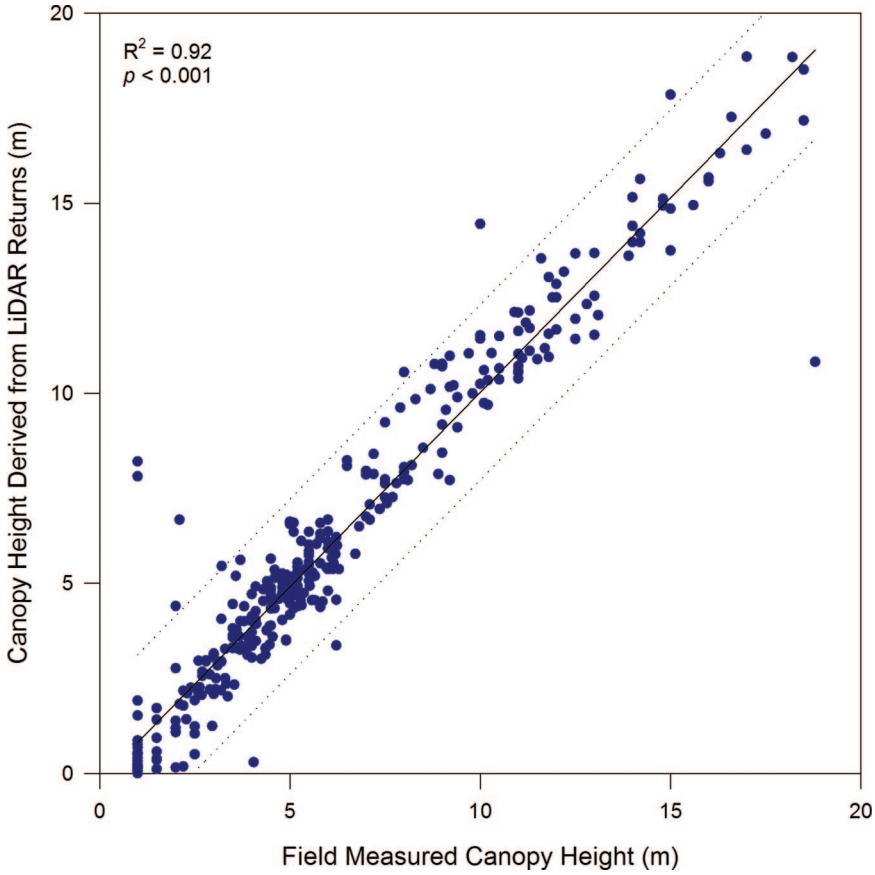

Fig. S3. Field validation of woody canopy height from 350 randomly selected points measured throughout KNP during the mapping campaign in April–May 2008.

Table S1. Descriptions of 4 large-scale herbivore treatments in KNP

Site	Age, years	Ecosystem	Substrate	Precipitation, mm year^{-1}	Area, ha	Fire return interval since establishment, years
Nwashitsumbe	41*	Northern plains	Basalt	425	230 (302)*	4.0†
Hlangwine	36	Southern hills	Granite	625	220	3.6†
Nkuhlu	6	Sabie River hillslope	Granite	525	139	n/a‡
Letaba	6	Letaba River hillslope	Granite	475	129	n/a‡

*The Nwashitsumbe exclosure was extended by 72 ha into the lowland habitat in 1986, providing a total of 302 ha for our analysis.
†Calculated from the KNP GIS database (http://www.sanparks.org/parks/kruger/conservation/scientific/gis/gisrsdataview.php)
‡A portion of Nkuhlu was burned in 2002 and 2007, but this portion was excluded from the study, leaving the analysis without fire as a covariate. Letaba has not been burned since the treatment was established in 2002.

Table S2. Height of woody canopies across the 4 treatment landscapes in both lowland and upland topographic positions in KNP

Site		Protected, m	Accessible, m
Long-term basalt (Nwashitsumbe)	Upland	2.6 ± 2.1	1.7 ± 1.2
	Lowland	3.3 ± 1.7	1.6 ± 1.4
Long-term granite (Hlangwine)	Upland	3.9 ± 2.0*	3.9 ± 2.2*
	Lowland	3.4 ± 2.5*	3.4 ± 2.5*
Short-term granite (Nkuhlu)	Upland	3.5 ± 2.3	3.0 ± 2.1
	Lowland	3.1 ± 2.2	3.0 ± 2.0
Short-term granite (Letaba)	Upland	2.2 ± 1.3*	2.2 ± 1.1*
	Lowland	4.6 ± 2.8	3.4 ± 2.4
Hillslope comparison	Upland	2.9 ± 2.0	2.7 ± 2.1
	Lowland	3.5 ± 2.3	2.7 ± 2.2
Total		3.3 ± 2.2	2.7 ± 2.1

*No significant difference in mean height between protected and accessible areas ($P < .05$; t test; $n = 27{,}000$).
"Protected" and "accessible" indicate portions of the landscape without and with herbivore activity, respectively. Canopy height values are the mean canopy height ± SD derived from airborne laser returns.